

# Designing Reverse Electrodialysis Process for Salinity Gradient Power Generation via Disjunctive Programming

Carolina Tristán<sup>a</sup>, Marcos Fallanza<sup>b</sup>, Raquel Ibáñez<sup>b</sup>, Ignacio E. Grossmann<sup>c</sup> and David Bernal Neira<sup>a,d,e\*</sup>

<sup>a</sup> Purdue University, Davidson School of Chemical Engineering, West Lafayette, IN, USA

<sup>b</sup> University of Cantabria, Department of Chemical and Biomolecular Engineering, Santander, Spain

<sup>c</sup> Carnegie Mellon University, Department of Chemical Engineering, Pittsburgh, PA, USA

<sup>d</sup> Universities Space Research Association, Research Institute of Advanced Computer Science, Mountain View, CA, USA

<sup>e</sup> Quantum Artificial Intelligence Laboratory, NASA Ames Research Center, Moffett Field, CA, USA

\* Corresponding Author: [dbernaln@purdue.edu](mailto:dbernaln@purdue.edu).

## ABSTRACT

Reverse electrodialysis (RED) is a nascent renewable technology that generates clean, baseload electricity from salinity differences between two water streams, a renewable source known as salinity gradient energy (SGE). Full-scale RED progress calls for robust techno-economic and environmental assessments. Using generalized disjunctive programming (GDP) and life cycle assessment (LCA) principles, this work proposes cost-optimal and sustainable RED process designs involving different RED stack sizes and width-over-length ratios to guide the design and operation from the demonstration to full-scale phases. Results indicate that RED units will benefit from larger aspect ratios with a relative increase in net power of over 30% with 6 m<sup>2</sup> membrane size. Commercial RED unit sizes (0.25–3 m<sup>2</sup>) require larger aspect ratios to reach an equal relative increase in net power but exhibit higher power densities. The GDP model devises profitable RED process designs for all the assessed aspect ratios in a foreseeable scenario for full-scale deployment, that is, the energy recovery from desalination concentrates mixed with reclaimed wastewater effluents. A RED system with 3 m<sup>2</sup> RED units nine times wider than its length could earn a net present value of \$2M at a competitive levelized cost of electricity of \$111/MWh in the Spanish electricity market. On-site, RED-based electricity could abate roughly 7% of the greenhouse gas emissions from the desalination plant's energy supply, given the low emissions contribution of RED supply share. These findings demonstrate that optimization-based eco-technoeconomic assessments are a vital ally in making RED a full-scale reality.

**Keywords:** Process Design, Renewable and Sustainable Energy, Optimization, Pyomo, Modelling and Simulations, Life Cycle Analysis

## INTRODUCTION

Demonstrating and deploying clean renewable energy technologies must be a global priority in pursuing a net-zero emissions economy by mid-century [1]. Salinity gradient energy (SGE) technologies offer deep and sustained reductions in greenhouse gas (GHG) emissions to keep the 2050 goal within reach. These technologies recover the chemical energy released when high-salinity and low-salinity streams are reversibly mixed. Reverse electrodialysis (RED) is one of the most researched and advanced SGE technologies.

RED employs ion-exchange membranes (IEMs) to generate electricity from SGE directly. These IEMs allow ions of opposite charge but not water to pass through. A RED device is built by stacking a series of alternating cation (CEMs) and anion exchange membranes (AEMs) that separate salt solutions of different concentrations. Selective transport of ions through the IEMs creates an electric potential across the pairs of AEMs and CEMs that drive redox reactions at electrodes on either side of the membrane pile. The overall electric potential of the set of cell pairs and the electric current then power an external load that closes the circuit [2].

In 2014, REDstack BV hit a significant milestone when their demonstration plant was successfully put into operation on the Afsluitdijk in the Netherlands, meeting Technology Readiness Level (TRL) 7. With a total membrane area per stack of 250 m<sup>2</sup>, this plant is powered by a blend of salt water and freshwater, producing 50 kW at present [3,4]. The REAPower pilot plant in Trapani, Italy is not functioning now and is being used as a demonstration project. Using both natural saturated brine from a saltworks and brackish water from a shoreline well, a trio of RED stacks were able to generate a total power output of 330 W, with a combined membrane area of more than 400 m<sup>2</sup> [5]. The main barriers preventing RED technological readiness are the low power density of large-scale RED systems (0.38–2.7 W/m<sup>2</sup> total membrane area), fouling, and the high cost of commercial membranes (> \$100/m<sup>2</sup>) [6–8]. The development of high-performing membranes, electrode segmentation, and multi-staging are some of the approaches to enhance the power density and energy efficiency of RED.

The water sector opens new avenues to prove and advance full-scale RED. Desalination concentrates and treated wastewater effluents are abundant yet largely untapped waste streams from which RED can extract sustainable and clean electricity [9]. On-site RED electricity generation in desalination plants can also lessen the dependence on the water and energy-intensive grid mix and reduce the environmental burden and costs associated with brine treatment and disposal [10]. This, in turn, contributes to more sustainable and self-sufficient water supply systems. Besides, RED operation with desalination brines delivers higher power densities than river/seawater pairs, and the reject brine does not require further energy-intensive treatment as raw seawater.

Even so, the complex process configuration and operational decision space make it technically challenging to estimate the costs and performance of RED with conventional heuristics. In previous work, we developed a Generalized Disjunctive Programming (GDP) optimization model incorporating a RED stack predictive model to define the cost-optimal RED process design in different scenarios [11]. The solution for the GDP model provided the flowsheet design that maximizes the process net present value (NPV) for a given RED stack design.

The quantification of the RED process environmental loads is also a valuable input to devise environmentally sound design alternatives to RED technology. In this regard, we conducted a life cycle assessment (LCA) of the RED stack to define the environmental profile of RED and to estimate greenhouse gas (GHG) emissions reduction in desalination plants partly sourced with SGE [12].

Building on the LCA of the RED unit and the GDP optimization model of the RED process, this follow-up work explores how scaling up and the design of the RED units' compartments may affect the eco-technoeconomic performance of the optimal RED process flowsheets.

## METHODS

The performance metrics in the eco-techno-economic assessment (eTEA) are the net power output (NP), the net power density (NPD, i.e., net power per total membrane area), the NPV, the levelized cost of electricity (LCOE), and the global warming potential (GWP).

### Problem Statement

Given a set of identical candidate RED units  $r \in RU = \{r1, \dots, rN_r\}$ , the goal is to determine which ones are active, how they are hydraulically arranged, and their working conditions (*e.g.*, electric current, inlet flow rate, and molar concentration of the HC and LC streams) that yield the cost-optimal flowsheet design of the RED process for a given concentration, volume, and temperature of the high-salinity and low-salinity feed streams, and design parameters of the RED units.

The superstructure in Figure 1 incorporates all the alternative hydraulic topologies for the RED system with  $N_r$  conditional RED units. The superstructure and notation are fully described in previous work [11].

Table 1 summarizes the design parameters of the RED units spanning pilot to commercial scales and different compartment geometries. We set seven distinct sizes (active area in Table 1) and, for each size, nine different width-over-length ratios (aspect ratio, Table 1). Using the predictive model, we estimate the operational conditions that maximize the net power of the stand-alone RED unit for each size and aspect ratio. This sensitivity analysis provides guidelines for RED unit design and operation in all development stages.

We quantify the GWP of the RED units in Table 1 based on the previous LCA of pilot-scale RED units [12].

Later, to explore how the design of the RED stack compartments affects the techno-economic and environmental performance of the optimal RED process design, we solve the GDP model of the RED system with 3 m<sup>2</sup> size RED units varying their aspect ratio.

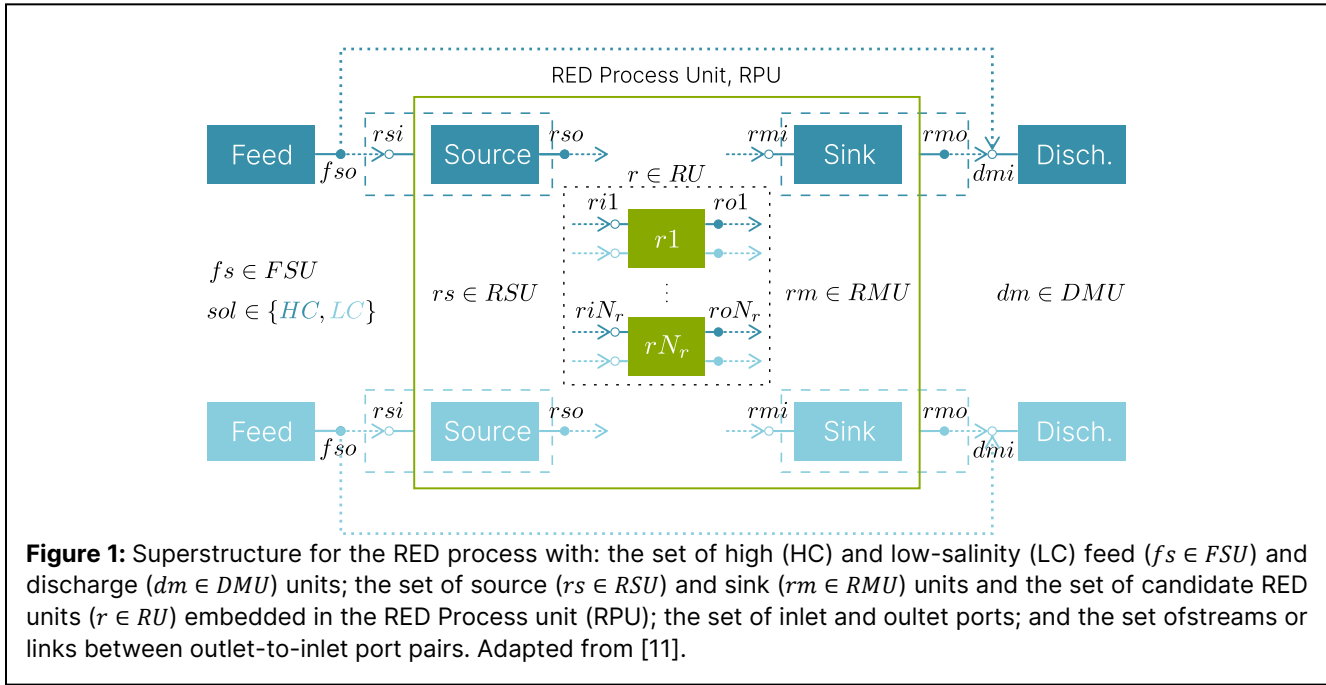


**Figure 1:** Superstructure for the RED process with: the set of high (HC) and low-salinity (LC) feed ( $f_s \in FSU$ ) and discharge ( $dm \in DMU$ ) units; the set of source ( $rs \in RSU$ ) and sink ( $rm \in RMU$ ) units and the set of candidate RED units ( $r \in RU$ ) embedded in the RED Process unit (RPU); the set of inlet and outlet ports; and the set of streams or links between outlet-to-inlet port pairs. Adapted from [11].

**Table 1:** Design parameters of the RED stack [11].

Parameter	Value
Number of cell pairs	1000
Aspect ratio, w/L	1–9
Active area	0.25, 1, 2, 3, 4, 5, 6 m <sup>2</sup>
<b>Spacers</b>	
Thickness	270 μm
Porosity	82.5%
<b>IEM: fumasep® CEM (FKS-50) / AEM (FAS-50)</b>	
Areal resistance	1.8 / 0.6 Ω/cm <sup>2</sup>
Permselectivity	0.93
Thickness	50 μm

## Optimization Model

The set of equations (1) defines the general form of the Generalized Disjunctive Programming (GDP) optimization model for the superstructure in Figure 1.

We code the GDP model using the algebraic modeling language Pyomo [13] and Pyomo.GDP [14], a dedicated Pyomo library extension for logic-based modeling and optimization.

$$\begin{aligned}
 \max NPV &= f(x) \\
 \text{s. t. } &g(x) \leq 0 \\
 &\begin{bmatrix} Y_r \\ h_r(x) \leq 0 \end{bmatrix} \vee \begin{bmatrix} \neg Y_r \\ B^r x = 0 \end{bmatrix} \quad \forall r \in RU \quad (1) \\
 &\Omega(Y_r) = True \\
 &x \in X \subseteq R^n \\
 &Y_r = \{True, False\} \quad \forall r \in RU
 \end{aligned}$$

In problem (1), the objective is to maximize the NPV of the RED process. The continuous variables  $x$  are the molar concentration and flow rate of the streams and the internal variables of the active RED units. The decision variables are the electric current, inlet concentration, and flow rate of the RED stacks.

The global constraints,  $g(x) \leq 0$ , describe specifications and physical relationships that must hold for any selection of alternatives in the superstructure, *e.g.*, mass balances of the feed, source, sink, and discharge units, and concentration and flowrate upper and lower bounds.

The  $N_r$  two-term disjunctions denote the discrete activation and deactivation of the  $N_r$  candidate RED units governed by the corresponding Boolean variables  $Y_r$  in each disjunct. When the unit exists ( $Y_r = True$ ), the active constraints  $h_r(x) \leq 0$  impose the RED unit discretized model equations (*e.g.*, mass and energy balances or other physicochemical phenomena within the RED unit), compute the capital and operating costs, and set bounds on the internal variables and the concentration and flow rate of the inlet and outlet streams; otherwise, ( $\neg Y_r$ ) the RED unit equations in the inactive disjunct are ignored, and  $B^r x = 0$  constraints set to zero a subset of the continuous variables and cost terms in the objective function.

The logical relationships ( $\Omega(Y_r) = True$ ) establish the logic conditions for selecting the candidate RED units.

To formulate the GDP problem, we assume:

1. Pure sodium chloride (NaCl) feed solutions, thus presuming ideal aqueous solution (*i.e.*, unity activity coefficients) and the absence of other species.
2. The ionic resistances of solutions and membranes are the unique internal energy loss.

3. Constant membranes' permselectivity and ionic resistance with concentration and temperature.
4. No water transport across membranes due to osmosis, so the streamwise volumetric flow rate in the RED channel is constant.
5. Salt diffusivities in the membrane phase are independent of concentration and temperature.
6. No fluid leakage or ionic shortcut currents in the RED stack's manifolds.
7. Co-current flow.
8. Isothermal and isobaric conditions.

Be aware that simplifying the RED stack model [11] leads to an increased net power output, causing the LCOE to be underestimated and the NPV to be overestimated.

The NPV of the RED process (2) accounts for discounted annual revenues from electricity sales and carbon pricing incentives and discounted operating costs (OPEX in \$/year) and capital expenses (CAPEX in \$). The OPEX and annualized CAPEX define the total annual cost (3), TAC, of the RED system. The CAPEX is annualized over the expected lifetime of the plant  $LT$  in years, using the capital recovery factor,  $CRF$ , given in (4) with a discount rate  $DR$ .

We assume the RED plant electricity is sold to the grid at the Spanish average price of electricity for non-house consumers,  $ep$  [15], and that the abated GHG emissions from the grid mix (Spanish emission factor,  $ef$ ) are subsidized at the average price,  $cp$ , in the European Union Emission Trading System (EU ETS) [16].

$$NPV = \frac{(ep + cp ef) TNP - TAC}{CRF} \quad (2)$$

$$TAC = CRF CAPEX + OPEX \quad (3)$$

$$CRF = \frac{DR}{1 - (1 + DR)^{-LT}} \quad (4)$$

$$TNP = \sum_{r \in RU} NP_r \quad (5)$$

We adapt our RED stack model [10] for a tractable yet rigorous solution. When the RED unit is active ( $Y_r = True$ ), the discretized model computes the net power output,  $NP_r$ , that is added to the RED system net power capacity, *i.e.*, total net power,  $TNP$  in kW (5). The net power output equals zero when the RED unit is absent ( $\neg Y_r$ ).

We apply a load factor,  $LF$ , to the annual full-capacity energy yield (kWh/year) of the RED plant to account for plant downtime due to membrane cleaning and system maintenance.

The capital investment involves the cost of RED stacks,  $\sum_{r \in RU} CC_{stack,r}$ , pumps,  $CC_{pump}$ , and civil and electrical infrastructure costs,  $CC_{civil}$ .

$$CAPEX = \sum_{r \in RU} CC_{stack,r} + CC_{pump} + CC_{civil} \quad (6)$$

The annual operating cost comprises the electricity cost from pumps,  $\sum_{r \in RU} OC_{pump,r}$ , the replacement cost of membranes,  $\sum_{r \in RU} OC_{IEMsrep,r}$ , and maintenance and labor costs (2% of CAPEX).

$$OPEX = \sum_{r \in RU} OC_{pump,r} + \sum_{r \in RU} OC_{IEMsrep,r} + 0.02 CAPEX \quad (7)$$

When the RED unit is active,  $CC_{stack,r}$  is added to CAPEX, and  $OC_{pump,r}$  and  $OC_{IEMsrep}$  to the OPEX; if not, these terms take zero values.

The objective function in (2) is maximized subject to constraints in the GDP detailed in [11]. The main financial parameters are reported in Table 2.

## Solution Strategy

We solve the GDP problem with the Global Logic-based Outer Approximation (GLOA) algorithm [17,18] implemented in the logic-based solver GDPopt version 20.2.28 built on Pyomo.GDP. The GLOA algorithm decomposes the solution to the GDP into a sequence of mixed-integer linear programming (MILP) problems and reduced nonlinear programming (NLP) subproblems.

We solve the MILP master problems with CPLEX and the NLP subproblems with BARON setting the time limit at 1 hour and 1% optimality gap on a machine running Windows 10 (x64) with 6 cores processor (Intel® Core™ i7-8700 CPU @3.2 GHz) and 16 GB of RAM. We use the MINLP and NLP solver versions from GAMS 34.1.0.

**Table 2:** Financial parameters of the RED process.

Parameter	Value
Plant lifetime, $LT$ [19]	30 years
Membrane lifetime [19]	10 years
Membrane price [20]	\$10/m <sup>2</sup>
Load factor, $LF$ [19]	90%
Discount rate, $DR$ [19]	5%
Spanish GWP, $ef$	0.374 kg CO <sub>2</sub> -eq/kWh
Carbon price, $cp$	\$27.8/t CO <sub>2</sub> -eq
Electricity price, $ep$	\$197/MWh

Spanish 2019-average price of electricity for non-house consumers. Band IB: annual consumption between 20 MWh and 500 MWh, excluding taxes and levies.

## RESULTS AND DISCUSSION

In all the assessments the RED units retrieve energy from the concentrate effluent of the Maspalomas II sea-water reverse osmosis desalination plant in Gran Canaria (Canary Islands, Spain) [21–23]. Maspalomas II plant rejects 17,602 m<sup>3</sup>/day (733 m<sup>3</sup>/h) of brine (1.67 M NaCl, 20°C) and consumes 3.77 kWh per cubic meter of desalted water. The low-salinity feedwater (20mM NaCl) is obtained from nearby wastewater treatment plants (*e.g.*, el Tablero, las Burras) [24], so the same LC and HC feed volume is available for SGE conversion.

### Stand-alone RED unit

The discretized RED unit NLP model involves 107–1187 variables and 107–1232 constraints is solved in 237 s up to an hour CPU time with BARON depending on the number of finite elements (from 3 up to 48 finite elements) that is set to keep the same axial discretization accuracy between the different sizes and aspect ratios.

Pilot-scale research often employs stack designs based on their counterparts in desalination, *i.e.*, electro-dialysis [6,25]. These modules feature greater length and smaller width, as the objective is to dilute the feed to comply with a given quality standard [26]. Alternatively, square geometries are usually adopted [5,6].

The premise of this study is that using modules that are wider than longer (*i.e.*, aspect ratio greater than one) while housing the same membrane area would allow more powerful systems and the treatment of larger feed volumes with fewer units. This would result in more compact and cost-effective systems.

The RED unit power generation sensitivity to aspect ratio increases with size (Figure 2). The smaller units require larger aspect ratios to reach an equal relative increase in NP. For instance, 1 m<sup>2</sup> units reach a 13% relative increase in NP when the aspect ratio moves from 1:1 to 9:1, while a RED unit twice its size requires a 4:1 ratio to reach the same increase. Increasing the width of the largest 6 m<sup>2</sup> stack nine times would lead to a 31% boost in net power generation, from 24.6 kW to 32.2 kW. In comparison, the smaller unit with an area of 0.25 m<sup>2</sup> and the same shape only generates 6% more net power than the square one.

Findings also indicate that while the largest RED unit delivers more net power than its pilot counterparts (Figure 2), it exhibits a lower power density (Figure 3). This may raise the cost per kWh of the RED unit despite the improvement in net power output.

Depending on the stack's geometry and size, and ultimately its ability to sustain the salinity gradient along the flow path, the optimal solution tunes the linear flow velocity in the HC and LC channels, the inlet concentration of the LC feedstream, and the electric current of the RED unit to maximize the net power output.

Shorter flow paths—realized by reducing the size for a given aspect ratio or increasing the aspect ratio for a given size—keep the inlet concentration gradient, *i.e.*, the highest driving force, along the channels. If the length is enlarged, there is enough time for ions to flow from the HC to the LC side, fading the concentration gradient.

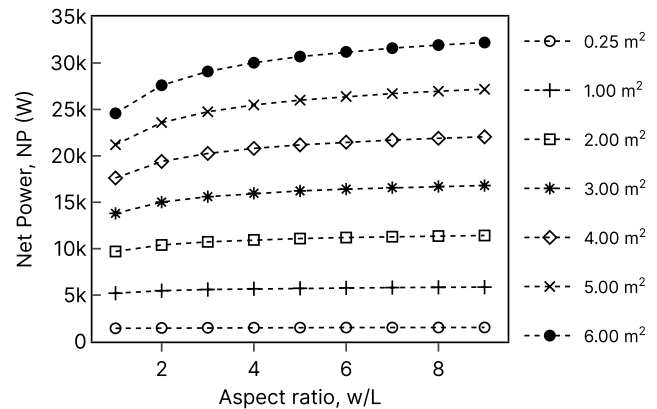


**Figure 2:** Optimal net power output of the stand-alone RED unit with different sizes (active area) and width-over-length ratios.

Recovering energy from high salinity gradients gives rise to two opposing effects on power generation. On one hand, the electric potential of the cell pairs increases, resulting in a higher gross power generation. On the other hand, the low conductivity of the LC channel increases the internal losses, leading to a decrease in gross power.

Given that the electric current drives the migration of ions across membranes from high-salinity to low-salinity compartments, the optimal electric current should decrease with longer RED units to extend the concentration gradient along the flow path. The opposite is true for shorter RED units, where the optimal solution sets a higher electric current, balancing the increase in the electric potential and internal resistance loss that arises from a higher concentration gradient, as shown in Table 3.

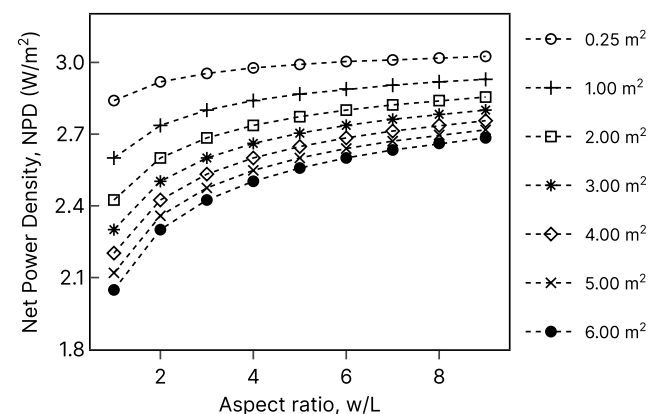


**Figure 3:** Net power density of the stand-alone RED unit with different sizes (active area) and width-over-length ratios under optimal net power conditions.

**Table 3:** Optimal operation variables of the 3 m<sup>2</sup> stand-alone RED unit.

		Aspect Ratio, w/L			
		1:1	3:1	6:1	9:1
Current density		7.64 mA/cm <sup>2</sup>	8.08 mA/cm <sup>2</sup>	8.26 mA/cm <sup>2</sup>	8.35 mA/cm <sup>2</sup>
Potential per cp		68.76 mV	69.94 mV	70.43 mV	70.65 mV
Linear velocity	HC	2.9 cm/s	2.5 cm/s	2.2 cm/s	2.1 cm/s
	LC	4.8 cm/s	3.9 cm/s	3.4 cm/s	3.1 cm/s
Flow rate	HC	40.66 m <sup>3</sup> /h	59.88 m <sup>3</sup> /h	76.08 m <sup>3</sup> /h	87.40 m <sup>3</sup> /h
	LC	66.53 m <sup>3</sup> /h	94.43 m <sup>3</sup> /h	116.15 m <sup>3</sup> /h	130.72 m <sup>3</sup> /h
LC Concentration		29 mM	37 mM	42 mM	44 mM
Net power, NP		13.8 kW	15.6 kW	16.4 kW	16.8 kW
Net Power Density, NPD		2.30 W/m <sup>2</sup>	2.60 W/m <sup>2</sup>	2.74 W/m <sup>2</sup>	2.80 W/m <sup>2</sup>

**Table 4:** NPV-optimal solution of the RED process with 3 m<sup>2</sup> RED units and different width-over-length ratios.

		Aspect Ratio, w/L			
		1:1	3:1	6:1	9:1
Active RED units		22	21	22	21
Net Present Value, NPV		\$1.8M	\$2.3M	\$2.5M	\$2.6M
Net Power Capacity, TNP		267 kW	274 kW	286 kW	282 kW
Net Power Density, NPD		2.02 W/m <sup>2</sup>	2.17 W/m <sup>2</sup>	2.16 W/m <sup>2</sup>	2.24 W/m <sup>2</sup>
Levelized Cost of Electricity, LCOE		\$132/MWh	\$116/MWh	\$114/MWh	\$111/MWh
Global Warming Potential, GWP		2.93	2.73	2.74	2.65
		kg CO <sub>2</sub> /MWh	kg CO <sub>2</sub> /MWh	kg CO <sub>2</sub> /MWh	kg CO <sub>2</sub> /MWh
# variables		24,249	15,849	12,249	10,449
# constraints		25,093	16,343	12,593	10,718

As the optimization model predicts, shifting to a wider-than-long stack design allows preserving the salinity gradient along the flow path with a lower linear velocity in the compartments. This, in turn, reduces hydraulic losses and pumping power to overcome head losses. Table 3 highlights the impact of this effect on the module with a membrane area of 3 m<sup>2</sup>. As the module length decreases, a downward trend in the optimal linear velocity is observed in both the HC and the LC. The flow rate rises despite the lower linear velocity due to the larger cross-sectional area. Concurrently, the concentration of the LC feed increases to offset the rise in the internal resistance.

### Optimal RED process design

We assume the superstructure has 25 identical candidate RED units with an active membrane area of 3 m<sup>2</sup>. For each aspect ratio (*i.e.*, 1, 3, 6, and 9) and the given financial parameters, the optimal solution provides the topology and decision variables that balance electricity production and capital and operating expenses. Discrete decisions involve the working RED units and the active water streams. Continuous variables are the inlet streams flow rate and concentration and active RED stacks electric current.

The GDP model finds profitable RED process designs for all the assessed RED units' aspect ratios (Table 4). But wider-than-long RED units earn more profits than the square peers with almost the same number of active RED units. As anticipated in the former section, the shorter RED stacks exhibit a higher power density. If the total membrane area and HC and LC feed volumes are the same, the RED process using shorter units can produce more power. In the NPV-optimal solution, to accommodate more wider-than-long RED units, the optimal solution makes them operate with flow rates below the optimal ones in Table 3. Such reduced inlet flowrate declines the RED units' net power density. Nevertheless, the increase in electricity production revenues considerably outstrips the increase in capital and operating cost of the wider-than-long RED units with lower power density.

By incorporating RED-based electricity, the grid mix share of the desalination plant supply could be decreased by as much as 7%, thereby reducing GHG emissions. This results from RED's relative emissions contribution to the energy supply being perceptibly slighter, at 2.6–2.9 kg CO<sub>2</sub>-eq/MWh compared to the Spanish grid mix, which emits 374 kg CO<sub>2</sub>-eq/MWh.

Overall, the GDP model defines cost-effective and sustainable RED process designs that improve the environmental profile and resource circularity of energy-intensive desalination and wastewater treatment plants; however, the nonconvexities leads to GDP problems that takes hours to solve with conventional global solvers (Table 4). This may be particularly true in full-scale RED systems with large-scale RED units.

## CONCLUSIONS

This work provides environmentally sustainable and cost-effective RED process designs exploring the RED units' different sizes and aspect ratios based on mathematical programming and the LCA framework. As a case study, we define energy recovery from mixing a real desalination plant's brine with reclaimed wastewater treatment plant effluents, a promising scenario for full-scale RED implementation.

The technical assessment of the size and different width-over-length ratios gives design and operation guidelines to derive compact systems that treat larger feed volumes with fewer yet powerful RED units. The assessment can assist in identifying the best aspect ratio for each module size.

Regarding the NPV-optimal RED process design with 3 m<sup>2</sup> RED units, the 9:1 width-over-length ratio yields the highest profit, \$2M, with an LCOE of \$111/MWh below the Spanish electricity market price (\$197/MWh) and a net power capacity of 282 kW from 22 RED units and virtually no added emissions to desalination plant's energy supply. As a result, RED-based electricity can abate around 7% of desalination plant's GHG from the grid mix supply at a competitive cost.

Overall, these results indicate that fine-tuning the aspect ratio is an effective way to advance in the development and commercial deployment of RED technology and prove that optimization-based eTEA is a robust tool to assist all development stages of emerging technologies such as RED electricity production.

Nonconvexities in the mixers and the RED unit model led to multiple optimal local solutions, therefore requiring computationally demanding global optimization techniques to solve to global optimality. This is particularly true, in large-scale RED systems where the model size significantly grows. A natural progression of this work is to reformulate the nonlinear equations into quadratic or linear approximations to exploit the bilinear nature of the GDP problem that solvers like Gurobi may effectively solve.

## ACKNOWLEDGEMENTS

The authors gratefully acknowledge the financial support from projects TED2021-129874B-I00 and PDC2021-120786-I00 through European Union NextGenerationEU/PRTR and MCIN/AEI/10.13039/501100011033.

Carolina Tristán acknowledges the financial support from the research fellowship PRE2018-086454 funded by the Spanish Ministry of Science and Innovation (MCIN/AEI/ 10.13039/501100011033) and "ESF Investing in your future".

David Bernal was supported by the NASA Academic Mission Services, Contract No. NNA16BD14C.

David Bernal and Carolina Tristán acknowledge the support of the startup grant of the Davidson School of Chemical Engineering at Purdue University.

## REFERENCES

1. International Energy Agency, Net Zero by 2050: A Roadmap for the Global Energy Sector, 2021.
2. Pattle R.E., Production of Electric Power by mixing Fresh and Salt Water in the Hydroelectric Pile, *Nature*. 174:660–660 (1954)
3. Post J.W., Goeting C.H., Valk J., Goinga S., Veerman J., Hamelers H.V.M., Hack P.J.F.M., Towards implementation of reverse electrodialysis for power generation from salinity gradients, *Desalin. Water Treat.* 16: 182–193 (2010)
4. IEA-OES, Annual Report: An Overview of Ocean Energy Activities in 2022, (2023).
5. Tedesco M., Cipollina A., Tamburini A., Micale G., Towards 1 kW power production in a reverse electrodialysis pilot plant with saline waters and concentrated brines, *J. Memb. Sci.* 522:226–236 (2017)
6. Tufa R.A., Pawlowski S., Veerman J., Bouzek K., Fontananova E., di Profio G., Velizarov S., Goulão Crespo J., Nijmeijer K., Curcio E., Progress and prospects in reverse electrodialysis for salinity gradient energy conversion and storage, *Appl. Energy* 225:290–331 (2018)
7. Chae S., Kim H., Gi Hong J., Jang J., Higa M., Pishnamazi M., Choi J.Y., Chandula Walgama R., Bae C., Kim I.S., Park J.S., Clean power generation from salinity gradient using reverse electrodialysis technologies: Recent advances, bottlenecks, and future direction, *Chem. Eng. J.* 452:139482 (2023)
8. Nazif A., Karkhanechi H., Saljoughi E., Mousavi S.M., Matsuyama H., Recent progress in membrane development, affecting parameters, and applications of reverse electrodialysis: A review, *J. Water Process Eng.* 47:102706 (2022)

9. Rani A., Snyder S.W., Kim H., Lei Z., Pan S.Y., Pathways to a net-zero-carbon water sector through energy-extracting wastewater technologies, *Npj Clean Water* 5:49 (2022)
10. Tristán C., Fallanza M., Ibáñez R., Ortiz I., Recovery of salinity gradient energy in desalination plants by reverse electrodialysis, *Desalination* 496:114699 (2020)
11. Tristán C., Fallanza M., Ibáñez R., Ortiz I., Grossmann I.E., A generalized disjunctive programming model for the optimal design of reverse electrodialysis process for salinity gradient-based power generation, *Comput. Chem. Eng.* 174:108196 (2023)
12. Tristán C., Rumayor M., Dominguez-Ramos A., Fallanza M., Ibáñez R., Ortiz I., Life cycle assessment of salinity gradient energy recovery by reverse electrodialysis in a seawater reverse osmosis desalination plant, *Sustain. Energy Fuels*. 4:4273–4284 (2020)
13. Hart W.E., Laird C.D., Watson J.-P., Woodruff D.L., Hackebeil G.A., Nicholson B.L., Siirola J.D., Pyomo — Optimization Modeling in Python, Second Edi, Springer International Publishing, Cham, (2017)
14. Chen Q., Johnson E.S., Bernal D.E., Valentin R., Kale S., Bates J., Siirola J.D., Grossmann I.E., Pyomo.GDP: an ecosystem for logic-based modeling and optimization development, *Optim. Eng.* 23:607–642 (2022)
15. EUROSTAT, Electricity prices for non-household consumers - bi-annual data (from 2007 onwards) [NRG\_PC\_205], (n.d.).  
<https://ec.europa.eu/eurostat/databrowser/bookmark/65f83096-1534-4ddc-a561-44764c07601c?lang=en>
16. ICAP, Allowance Price Explorer, (2022).  
<https://icapcarbonaction.com/en/ets-prices>
17. Lee S., Grossmann I.E., A global optimization algorithm for nonconvex generalized disjunctive programming and applications to process systems, *Comput. Chem. Eng.* 25:1675–1697 (2001)
18. Chen Q., Johnson E.S., Siirola J.D., Grossmann I.E., Pyomo.GDP: Disjunctive Models in Python, *Comput. Aided Chem. Eng.* 44: 889–894 (2018)
19. Giacalone F., Papapetrou M., Kosmadakis G., Tamburini A., Micale G., Cipollina A., Application of reverse electrodialysis to site-specific types of saline solutions: A techno-economic assessment, *Energy*. 181:532–547 (2019)
20. Small Business Innovation Research (SBIR) and Small Business Technology Transfer (STTR) programs, Low-Cost Manufacturing of High-Performance Ion Exchange Membranes for Electrodialysis using Initiated Chemical Vapor Deposition, (n.d.).  
<https://www.sbir.gov/node/2282063>
21. Meyer-Steele S., von Gottberg A., Talavera J.L., New Sea Water Reverse Osmosis Plant for the Caribbean "Energy Recovery, Brine Recovery & Cost Reduction" Ionics Technical Paper (2001)
22. Portillo E., de la Rosa M.R., Louzara G., Quesada J., Ruiz J.M., Mendoza H., Dispersion of desalination plant brine discharge under varied hydrodynamic conditions in the south of Gran Canaria, *Desalin. Water Treat.* 52:164–177 (2014)
23. Sadhwani Alonso J.J., Melián-Martel N., Environmental Regulations—Inland and Coastal Desalination Case Studies. In: Sustainable Desalination Handbook: Plant Selection, Design and Implementation, Ed: V.G. Gude, Butterworth-Heinemann (2018)
24. Pérez Talavera J., Quesada Ruiz J., Identification of the mixing processes in brine discharges carried out in Barranco del Toro Beach, south of Gran Canaria (Canary Islands), *Desalination*. 139:277–286 (2001)
25. Yasukawa M., Mehdizadeh S., Sakurada T., Abo T., Kuno M., Higa M., Power generation performance of a bench-scale reverse electrodialysis stack using wastewater discharged from sewage treatment and seawater reverse osmosis, *Desalination*. 491:114449 (2020)
26. Gurreri L., Tamburini A., Cipollina A., Micale G., Electrodialysis applications in wastewater treatment for environmental protection and resources recovery: A systematic review on progress and perspectives, *Membranes (Basel)*. 10:1–93 (2020)

© 2024 by the authors. Licensed to PSEcommunity.org and PSE Press. This is an open access article under the creative commons CC-BY-SA licensing terms. Credit must be given to creator and adaptations must be shared under the same terms. See <https://creativecommons.org/licenses/by-sa/4.0/>

